Polyethylenimine-based Magnetic Nanocomplexes Enhanced Cisplatin Toxicity on Ovarian Cancer Cells in Presence of Static Magnetic Field

Faranak Ashoori
Tarbiat Modares University Faculty of Biological Sciences
Behnam Hajipour-Verdom
Tarbiat Modares University Faculty of Biological Sciences
Mohammad Satari
University of Malayer
Parviz Abdolmaleki (parviz@modares.ac.ir)
Tarbiat Modares University Faculty of Biological Sciences https://orcid.org/0000-0003-4131-2919

Research

Keywords: Magnetic iron oxide nanoparticles, Cisplatin, Polyethylenimine, Cytotoxicity, Cell responses

Posted Date: January 5th, 2021

DOI: https://doi.org/10.21203/rs.3.rs-138892/v1

Abstract

Background

The drug resistance of cancer cells is a major problem in the chemotherapy. Cisplatin (CIS) is one of the most effective chemotherapeutics used for ovarian cancer. Resistance to different chemo-drugs has developed over times. Here, we investigated the experimental approach to increase the CIS cytotoxicity and overcoming cell resistance through nanoparticle-based combination treatments. Polyethylenimine (PEI)-based magnetic iron oxide nanocomplexes were used to transfer the drugs in both genetically matched CIS-resistant (A2780CP) and -sensitive (A2780) ovarian cancer cells in presence of 20 mT static magnetic field. Magnetic nanoparticles (MNPs) were synthesized and bonded to PEI cationic polymer that leads to formation of binary complexes (PM). In the following, binding of CIS to PM binary complexes two including ternary complexes PM/C (PEI-MNP/CIS) and PMC (PEI-MNP-CIS) formed.

Results

Our results showed that the CIS cytotoxicity increased at different concentrations of CIS and PEI in all of binary and ternary treatments overtimes. Furthermore, CIS induced S and G2/M phase's cell cycle arrest as well as reactive oxygen species (ROS) production in the both cell lines. Ternary complexes enhanced apoptosis more than binary complexes in the treated-cells.

Conclusions

PEI-based magnetic noncomplex can be considered as a novel carrier for increasing the CIS cytotoxicity and probably overcoming drug resistance in ovarian cancer cells.

Background

Disruption in the cell cycle progression impacts on the cell homeostasis and physiological functions that can leads to cancer. Ovarian cancer represents fourth diagnosed cancer among women population in the world and more than any other cancers that threaten the female reproductive system. Many risk factors identified for ovarian cancer such as lifetime ovulatory cycles and etc., (1,2). Ovarian cancer is the leading cause of death in gynecologic cancers through the tumor spreading beyond the ovary at the time of diagnosis (3).

Cisplatin (CIS) as platinating agents most generally used to chemotherapy a wide range of cancers such as breast, lung, ovarian cancer and etc., (4–6). This compound inhibits DNA synthesis through the binding to guanine base and forming intra-strand DNA adducts (7). The drug resistance is the most important problem in the CIS treatment of ovarian tumor cells that easily occur in the early phase of chemotherapy(8,9). Various mechanisms have been proposed for drug resistance containing genes caused to drug resistance such as cooper transporter protein (10–12). Another mechanism that leading to CIS drug resistance is related to multidrug resistance (MDR) protein, which pumps the drug to

extracellular with consumption of energy (13–17). Generally, CIS resistance can be accomplished by number of cellular adaptations including uptake decrement, inactivation by glutathione, metallothionein and other anti-oxidants, and also increasing the gene expression of DNA repairing system (13,18–20). There is an ongoing attempt to overcome the drug resistance because it is necessary for efficient treatments. Indeed, there is no an effective approach for overcoming of drug resistance in the cancer therapy (21–25).

Zhang et al., using the Hsp90 inhibitors reverse the CIS resistance by modifying the expression of multiple drug resistance related genes (26). In the another study, Ai et al., showed that inhibition of HIF-1α induces reactive oxygen species (ROS) overproduction in CIS-resistant cells and resensitizes CIS-resistant ovarian cancer cells (27). Moreover, Hu et al., found that targeted-nanocarriers are able to deliver drug, oligonucleotide, peptide and DNA to tumor cells through enhancing of permeation and retention effects. Nanoparticle-based combination approaches used in clinical assessment to overcome drug resistance including control of over drug loading, temporary sequencing on drug release and co-encapsulation of drugs by various physicochemical properties (28,29).

Studies demonstrated that curcumin-loaded nanoparticles induce apoptotic cell death through regulation of the MDR functions and ROS levels in CIS-resistant human ovarian cancer cells (30). Polyethylenimine (PEI) polymer has been used for transfer of gene, protein, and anticancer drugs (31–35). Yang et al., showed that chemo-radioresistance of glioblastoma was decreased using microRNA145 with cationic polyurethane-short branch PEI (PU-PEI), which is effectively suppressed the expression of drug-resistance and anti-apoptotic genes that consequently leads to a novel therapeutic approach for malignant brain tumors (36).

Magnetic fields (MFs) have effects on the biological systems and may increase the production of ROS, which may leads to oxidative stresses in the DNA, protein and lipids as well as cause genetic mutations, apoptosis cell death and etc., (37,38). Cell proliferation is impacted through treatments with both anticancer agents and MFs that enhance the anticancer effect of chemotherapeutics, which may serve as a novel combination approach in the cancer therapy (38). In this study, we examined the magnetic iron oxide nanoparticles (MNPs) with PEI cationic polymer to increase the CIS cytotoxicity and overcome drug-resistance. These drug-loaded PEI-based MNPs were transferred by homogenous static magnetic field (SMF) into sensitive and resistant ovarian cancer cell lines. PEI-based magnetic nanocomplexes can boosted the drug delivery as well as cytotoxicity, and may decreased the cell drug resistance.

Results

Formation of magnetic nanoparticles

As results as shown in **Fig. 1**, the FTIR spectrum of MNPs indicated on two peaks. The first absorption is at 3420 cm^{-1}, which is related to the hydration bond formed with hydroxyl groups and the second absorption is at 572 cm^{-1}, which is due to vibrational band of Fe-O in MNPs. These peaks confirm the

accuracy of MNPs synthesis. In the PM binary complex IR spectrum, in addition to MNPs peaks, 2924, 1633, and 1029 cm^{-1} wavelengths indicate C-H, C-C, and C-N bonds of PEI polymer, respectively that confirmed the accuracy of PM binary complex formation. The FTIR spectrum of PMC ternary complexes, peaks at 867 cm^{-1} wavelength in addition to the peaks of MNPs and PM show the N-H bond of CIS in conjugation with other molecules were less than 500 cm^{-1}, which was not visible in our spectrum (41). Furthermore, the results of DLS as presented in **Table 1** showed the size corresponding of MNPs ~ 69 ± 5 nm, PM binary complex ~ 88 ± 15 nm and PMC ternary complex ~ 151 ± 21 nm, respectively, which seems that is suitable as delivery agents. Furthermore, zeta potential results indicated that the MNPs surface charge was about -25 eV, which negative surface charges create an interconnection through electrostatic interaction with positive charges of PEI.

Determination the cytotoxicity of cisplatin-conjugated magnetic nanoparticles

We assessed the cell viability of A2780/CP and A2780 cells in the different treatments at 24 and 48 h following the end point of treatments using MTT staining and microplate reader. As shown in **Fig. 2a, b**, CIS decreased the cell viability of A2780 compared to A2780/CP cells at the 48 h higher than 24 h, respectively. In addition, PEI can significantly decreased the viability of both cells compared to untreated cells in the two exposure times (**Fig. 2c, d**). The combination effects of CIS and PEI were determined as seen in **Fig. 3,** so that PC binary complex significantly increased the cytotoxicity in the different concentrations in both cell lines. In following treatments, the effect of 20 mT SMF exposure was evaluated on the cell viability in treated to PM binary complex (**Fig. 4**). The results showed that MNPs just has been enable to decrease the cell viability in the PM complexes in presence of SMF.

The mass of PEI that used in the nanocomplexes is an important parameter. The mass ratio of PEI/CIS as shown in **Fig. 5**, at different concentrations of PEI and constant concentration of 2.5 µg/ml CIS that decreased the cell viability of A2780 more than A2780/CP cells. Indeed, PEI boosted the CIS toxicity in the both cells especially in A2780 cells at 48 h. Moreover, in the **Fig. 6**, results indicated that cytotoxicity of PM/C and PMC at mass ratio of 0.4 including 2.5 µg/ml of CIS, 1 µg/ml of PEI and 1 µg/ml MNPs enhanced in presence of 20 mT SMF in both cell lines. Furthermore, the effects of PMC on the cell viability were more than PM/C complexes in presence and absence of SMF. The IC_{50} values of CIS, PEI, PC, PM, PM/C and PMC were calculated in A2780/CP and A2780 cells at 24 and 48 h (**Table 2**). These results suggested that PMC complexes were more effective from PM/C complexes for the cytotoxicity effects of CIS.

Cisplatin increased intracellular ROS production

We measured the intracellular ROS accumulations of A2780/CP and A2780 cells in presence and absence of 20 mT SMF treated to CIS, PEI and ternary complexes (PM/C and PMC) at the same

concentration for 48 h through fluorescent probe DCFH-DA and flow cytometry **(Supplementary Fig. S1**). As shown in **Fig. 7**, ROS levels significantly increased in all of these treatments compared to untreated cells. Moreover, PM/C and PMC complexes induced increment of ROS production more than alone CIS-treated cells.

Cisplatin induced S and G2/M phase cell cycle arrest

We evaluated the cell cycle distribution of A2780/CP and A2780 cells in presence and absence of 20 mT SMF treated to CIS, PEI and ternary complexes (PM/C and PMC) at the same concentration of 2.5 μM CIS, 1 μM PEI and 1 μM MNP for 48 h through PI staining and flow cytometry **(Supplementary Fig. S2**). As shown in **Fig. 8**, SMF caused S phase arrest in A2780/CP and G2/M phase arrest in A2780 cells. CIS triggered S and G2/M phase arrest in the both cell lines. Furthermore, PEI led to G2/M arrest in presence of SMF-treated A2780 cells more than A2780/CP cells. Besides, PMC and PM/C treatments induced S and G2/M phase in presence of SMF in the both cell lines.

Cisplatin promoted apoptosis in cancer cells

We investigated the apoptosis rate of A2780/CP and A2780 cells in presence and absence of SMF (20 mT) treated to CIS, PEI and PM/C and PMC ternary complexes at the same concentration for 48 h through annexin/PI and flow cytometry **(Supplementary Fig. S3**). As seen in **Fig. 9**, SMF can modulated the induction of apoptotic cell death in the A2780 cells compared the A2780/CP cells. SMF do not show any changes in the levels of apoptosis in CIS and PEI treatments in both cell lines. The apoptosis rate significantly increased in the PMC and PM/C treatments compared to alone CIS and PEI treatments. The PMC ternary complex showed a high level of apoptosis more than other treatments in A2780 cell line. Indeed, PMC was more effective than PMC for inducing apoptosis cell death.

Discussion

This study aimed to investigate the effects of PEI-based magnetic nanocomplexes on ovarian cancer cells in presence of SMF, and the probably mechanisms of this effects. Cancers are caused by a series of mutations in the genes and changes in the cell physiology and functions. Here, the ternary complexes of CIS increased cytotoxicity and cell accumulation in S and G2/M phase's cell cycle as well as ROS production and apoptosis cell death (34). Many efforts made to use the polymeric nanocomplexes to increase the cytotoxicity and efficiency of delivery systems enhancing drug toxicity and overcome chemo-drug resistance. Tseng et al., reported that CIS-incorporated gelatin nanocomplexes can be used for cancer chemotherapy (46). Lipid and polymer-based nanoparticles siRNA delivery systems are also developed by Mainini et al., to cancer therapy (47). Polymeric nanoparticles synthesized based on host–guest interaction between β-cyclodextrin and benzimidazole used for liver cancer-targeted therapy and its ability to induce cell apoptosis was found to be remarkable (48). Lim et al., used redox-responsive polymeric nanocomplexes for delivery of cytotoxic protein and chemotherapeutics. They synthetized a

nanocomplexes including PEI cross-linked by oxaliplatin (IV) pro-drug to generate ROS in the cell. The ROS can stimulates the controlled-drug release and effects on of protein reactivity (49). We similarly synthetized a noncomplex including PEI cross-linked by CIS and MNPs as ternary complexes (PMC) and characterized by FTIR **(Fig. 1)** and DLS **(Table 1)**, which enhanced the CIS cytotoxicity and successfully overcome drug resistance. As shown in **Fig. 2**, CIS and PEI decreased the cell viability of A2780 more than A2780/CP cells. The cytotoxicity increased in the PC **(Fig. 3)** and PM **(Fig. 4)** binary complexes, and also finally PMC ternary complex **(Fig. 6)**. CIS causes cell death by conjugation and disrupt the nuclear (nDNA) and mitochondrial DNA (mtDNA), which inhibits transcription and replication of nDNA and mtDNA (50).

Cationic polymers bind to negatively charged proteins in the cells such as heat shock proteins, glutathione s-transferases, which are involved in apoptosis. This is the most important mechanism of toxicity by PEI polymers that may enhance the CIS cytotoxicity in the PC, PM and PMC complexes (51,52). Recently, Karimi et al., reported a usage of $CoFe_2O_4$/MNPs as an effective carrier for epirubicin anticancer drug delivery (53). As shown in **Fig. 7**, ROS production significantly increased in all of the treatments. In addition, PMC and PM/C complexes induced enhancement of ROS production more than CIS. Free radicals have essential roles in the cell physiological and proliferation processes in low levels. In contrast, high accumulation of ROS leads to oxidative damages in the cell components and cell death (13). Indeed, the platinum in CIS induces the ROS production and damages in DNA, proteins and lipids, and also ultimately promotes the apoptosis (54)(4 P). PEI polymer in the PMC and PM/C complexes inhibits a number of antioxidant enzymes such as glutathione s-transferases which is a ROS scavenger. That may cause the increase of ROS content and therefore induction of apoptosis.

CIS induced S and G2/M phase cell cycle cell accumulation in A2780/CP and A2780 cells. PEI led to G2/M arrest in presence of SMF-treated A2780 cells more than A2780/CP cells. PMC and PM/C treatments induced S and G2/M phase cell cycle arrest by decrease of cell population in G0 / G1 phase in presence of SMF in the both cell lines **(Fig. 8)**. Enhancement of ROS levels increase the oxidation of nucleotides in the nucleotide pool and DNA molecules. Free radicals cause a variety of damages, including single- or double-stranded breaks in DNA, and eventually activate proteins such phosphorylated form of checkpoint kinases ATM in the cells. The ATM phosphorylates the Cdc25, p53 and E2F1 and initiates the repair process or apoptosis in the damaged-cells that their inactivation induce G2/M phase's cell cycles arrest (55–58).

As seen in **Fig. 9**, the apoptosis rate significantly increased in the PMC and PM/C treatments compared to CIS and PEI, only. In addition, the PMC ternary complex showed a high level of apoptosis compared to other treatments in A2780 cell line. The PMC was more effective than PM/C for inducing apoptosis cell death. The PMC complexes induce apoptosis through two mechanisms to including inhibitory potential of PEI on negatively charged proteins and also CIS conjugated to PM that promoted the efficiency of drug's transfer by PMC complexes while the PM/C complexes used only the first mechanism.

Although SMF exposure did not show any effects on the CIS and PEI treatments but SMF influences on the cell functions in treatment of MNPs through a mechanical force that caused the penetration of the

cell membrane and induced more apoptosis (59).

In the PM/C complexes, first the PEI polymer and MNPs entered to the cell without CIS. The PEI polymer had enough opportunity to inhibit the negatively charged proteins. Drug resistance decreased by neutralizing some of them in A2780/CP cells. While, in the PMC complexes, all components entered to the cells at the same time, so the efficiency of PEI was less than PM/C complexes. In A2780 cells, negatively charged proteins did not exceed. Therefore, the changes of IC50 rate at CIS in A2780/CP cells was greater than A2780 cells as shown in **Table 2.**

Isoelectric pH of most proteins involved in CIS resistance is less than pH ~ 7.2. These proteins have negative charge in neutral pH, which makes them a good target for binding to PEI. As shown in **Table 3**, the net charge of proteins involved in pre-target resistance that is negative. One of these proteins is the glutathione S-transferase enzyme, which its expression increases in CIS resistance (60, 61). The net charge and isoelectric pH of this enzyme is 3 and 5.3, respectively. The glutathione S-transferase enzymes are important scavengers of ROS that inhibition of them induced ROS accumulation, G2/M phase cell cycle arrest and apoptosis (52,62). PEI can binds to these negative-charged enzymes (51). Other negative biological molecules such as mRNA can also be targets of polymer binding. So that, proteins that are highly expressed in CIS resistance have more mRNA content in the cytoplasm. It seems that PEI may inhibits the scavengers of ROS in pre-target mechanism and translation of drug resistance proteins. Furthermore, the high buffering and endosomal escape of PEI trigger to endocytosis transferring. Endosomal escape that is the entry of carrier into the nucleus before it is prematurely destroyed by endosomes and intracellular lysosomes (63,64). Therefore, PMC complexes had less presence in the cytoplasm of cells. These complexes less recognized by lysosome or multi-drug resistance mechnisms and also less exposed to antioxidants such as glutathione, metallothionein and etc. In conclusion, PEI-based magnetic nanocomplexes may be a novel strategy to enhance the CIS cytotoxicity and possibly overcome the drug resistance in cancer cells.

Methods

Chemical reagents

Roswell park memorial institute 1640 (RPMI-1640) medium and fetal bovine serum (FBS) were purchased from Gibco. Penicillin-streptomycin and trypsin-EDTA were obtained from Bioidea. Cisplatin was purchased from Oncotic Pharma production GmbH, Germany. 25 kDa branched polyethylenimine was obtained from Sigma-Aldrich. 2',7'-dichlorofluorescein diacetate (DCFDA) (ab113851) was purchased from Abcam. Propidium iodide (PI), ($4H_2O.FeCl_2$), ($6H_2O.FeCl_3$) and (NaOH) were obtained from Merck. Annexin V apoptosis detection kit was purchased from eBioscience, USA.

Synthesis and characterization of magnetic nanoparticles

The Fe_3O_4 MNPs synthesized by co-precipitation approach. Physical properties of nanoparticles and size-dependent parameters such as reaction temperature, pH of suspension, initial molar concentration were investigated (39). In this approach, nanoparticles synthesized from ($4H_2O.FeCl_2$), ($6H_2O.FeCl_3$) and (NaOH) with high purity and distilled water. The ($4H_2O.FeCl_2$) and ($6H_2O.FeCl_3$) solutions were mixed in the respective stoichiometry (i.e., ratio Fe (II):Fe (III) = 1:2) in presence of OH^- deposited through the following reaction in **equation (1)**.

$$Fe^{2+} + Fe^{3+} + 8OH^- \rightarrow Fe(OH)_2 + 2Fe(OH)_3 \rightarrow Fe_3O_4 + 4H_2O \qquad (1)$$

Distilled water was initially deoxygenated by ultrasonic transducer and nitrogen gas. Then, iron salts II and III were added. The NaOH solution was also deoxygenated by the ultrasonic apparatus. The 12 ml of saline solution was added to 120 ml of NaOH solution under nitrogen atmosphere, and the solution was homogenized for 10 h at 10,000 rpm for 30 min. After that, the particles were washed three times with distilled water and once with acetone, and dried under vacuum conditions (40,41).

The binary complexes (PEI-CIS (PC)) and PEI-MNPs (PM)) were synthesized at 37°C for 1 h. for formation of ternary complexes (PEI-MNP/CIS (PM/C)) CIS bounded to PM binary complexes. Moreover, PEI, MNP and CIS bounded together at the same time and (PEI-MNP-CIS (PMC)) ternary complexes were synthesized at 37°C for 1 h.

The accuracy of MNPs and formation of binary and ternary complexes were confirmed by the Fourier transform infrared spectroscopy (FTIR) and dynamic light scattering analysis. FTIR spectra was done for dried sample of MNP, PM binary and PMC ternary complexes by FTIR spectrometer (Thermo scientific NICOLET IR100) in wave range of 4000 - 400 cm^{-1} with a resolution of 4 cm^{-1}. In brief, the dried sample was placed on a silicon substrate transparent to infrared, and spectra were measured by transmittance method. Then, spectrums of synthesized products were plotted through Essential FTIR software. The size and surface charge distribution of PEI, MNP.PM and PMC ternary complexes in solutions and suspensions was determined using Dynamic light scattering (DLS Zeta Sizer, a nano-ZS model, UK). Briefly, 1 mg/ml solution of nanoparticles made in deionized-water and placed in the ultrasonic bath for 30 min. The sample was filtered with a 0.25 µm to remove larger and accumulated particles. Then, the particle size distribution and surface charge were analyzed by Zetasizer software (version 7.11).

Cell culture

The CIS-resistant human ovarian carcinoma A2780/CP and sensitive A2780 cells were obtained from National Cell Bank of Iran (NCBI). A2780/CP is a sub-line of A2780 that gained CIS resistance in the in vitro (27). The cells were allowed to grow in RPMI-1640 in the neutral PH (7.2–7.4) supplemented with 10% (v/v) heat-inactivated (50 °C, 30 min) fetal bovine serum (FBS) and 2 mM glutamine, 100 units/mL of penicillin and 100 mg/mL of streptomycin at 37 °C and 5% CO_2 in a humidified incubator. The cells

were trypsinized (0.025% trypsin, 0.02% EDTA) after they grown until 70–80% confluent. Prior to treatments, cells were allowed to reattach overnight.

Magnetic field exposure

We used permanent cobalt magnets to apply 20 millitesla (mT) homogenous SMF. The magnitude of this magnetic field was calculated by a Teslameter (13610.93, PHYWE, Gottingen, Germany) with a probe type of Hall Effect in respect to its cross-sectional area and thickness. We exposed 20 mT SMF to cells through placing magnets under bottom of cell culture plates during this study.

Cell treatments

The A2780/CP and A2780 cells were treated by CIS and PEI at concentrations of 5, 10, 25, 50 and 100 µg/ml, PC binary complex included concentrations of PEI (1, 2.5, 5 and 10 µg/ml) and CIS (2.5, 5, 7.5 µg/ml) and PM binary complex included concentrations of PEI (2.5, 5 and 10 µg/ml) and MNPs (1 µg/ml) in presence and absence of 20 mT SMF for 24 and 48 h. Moreover, cells were treated at mass ratio of PEI/CIS (0.4, 0.5, 1, 2 and 4 w/w) for 24 and 48 h. In addition, cells treated with PM/C and PMC ternary complexes at concentrations of 1 µg/ml PEI, 1 µg/ml MNPs and 2.5 µg/ml CIS in presence and absence of SMF for 48 h.

Cell viability assay

The cell viability of A2780/CP and A2780 cells were measured by tetrazolium-based colorimetric assay (MTT assay). Briefly, cells (10^4 cells/ well) were seeded into 96-well culture plate (SPL Life Sciences Co., Ltd. Korea) and incubated in a total volume of 100 µL supplemented RPMI at 37 °C and 5% CO2 in a humidified incubator. Cells were initially allowed to attach overnight. Following the treatments, 100 µL FBS-free RPMI containing of 0.5 mg/mL MTT was added to each well and kept at 37 °C for 4 h in the dark. Then, formazan was dissolved by 100 µL/well DMSO. The relative number of living cells in each group was measured by microplate reader (uQuant MQX200, BioTek, USA) at 570 nm. Cell viability results were shown as percentage compared to control cells. Sensitivity of selected cell types evaluated by the half-maximal inhibitory concentration (IC50).

Quantitation of intracellular ROS accumulation

Intracellular ROS levels under normal and stress conditions were detected using 2',7'–dichlorofuorescein diacetate (DCFDA) assay kit. The A2780/CP and A2780 cells were treated in 1 µg/ml of PEI and 2.5 µg/ml of CIS as well as PM/C and PMC complexes (at concentrations of 1 µg/ml of PEI, 1 µg/ml of MNP and 2.5 µg/ml of CIS) compared to untreated cells in the presence and absence of SMF for 48 h, which were prepared in supplemented RPMI media with 10% FBS in the 6-well cell culture plate (SPL Life

Sciences Co., Ltd. Korea). After treatments, cells were prepared immediately as recommended by the manufacturer. Briefly, the cells were washed with PBS. Then the samples were suspended in the conical test tube with 20 µM DCFDA in the 1X buffer and incubated at 37 °C in dark for 30–45 min. Measurement of ROS production was monitored immediately by FACScalibur Becton-Dickinson flow cytometry (Franklin Lakes, NJ). The DCFDA flow cytometric data were analyzed by flowjo software (version 7.6.1) (27,42,43).

Cell cycle analysis

The A2780/CP and A2780 cells were treated to 1 µg/ml of PEI and 2.5 µg/ml of CIS as well as PM/C and PMC complexes (at concentrations of 1 µg/ml of PEI, 1 µg/ml of MNP and 2.5 µg/ml of CIS) in presence and absence of SMF for 48 h, which were prepared in supplemented RPMI media with 10% FBS in the 6-well cell culture plate (SPL Life Sciences Co., Ltd. Korea) and incubated at 37 °C and 5% CO_2 in a humidified incubator. After that, cells were trypsinized and collected through centrifugation at 400g for 5 min. Then, cells were resuspend in 0.5 ml of PBS and fixed by adding 4.5 ml of 70% (v/v) cold ethanol, and centrifuged at 400g for 5 min. After that, cells were washed in 5 ml PBS, centrifuged at 400g for 5 min and incubate at room temperature for 5 min, and recentrifuged at 400g for 5 min, respectively. Then, supernatant was removed and resuspended in 1 ml of DNA staining solution. The prepared cells were incubated for at least 30 min at room temperature in the dark. The obtained cell suspension was analyzed by FACScalibur Becton-Dickinson flow cytometry (Franklin Lakes, NJ). Data were collected from at least 104 cells. The flow cytometric data were analyzed by flowjo software (version 7.6.1) (44).

Detection of cell apoptosis

Apoptosis was detected using annexin V-FITC/PI staining. The A2780/CP and A2780 cells were treated in 1 µg/ml of PEI and 2.5 µg/ml of CIS as well as PM/C and PMC complexes (at concentrations of 1 µg/ml of PEI, 1 µg/ml of MNPs and 2.5 µg/ml of CIS) in presence and absence of SMF for 48 h, which were prepared in supplemented RPMI media with 10% FBS in the 6-well cell culture plate (SPL Life Sciences Co., Ltd. Korea) and incubated at 37°C and 5% CO2 in a humidified incubator. After that, cells were collected and labeled by annexin V/PI in 1X binding buffer for 15 min. Then, the apoptotic and necrotic cells were evaluated by FACScalibur Becton-Dickinson flow cytometry (Franklin Lakes, NJ). The flow cytometric data were analyzed by flowjo software (version 7.6.1). Total number of apoptotic and necrotic cells were defined as sum of Annexin V+/PI-and Annexin V+/PI+ populations including Q1 = Necrosis; Q2 = Late Apoptosis; Q3 = Early Apoptosis; Q4 = Live Cells (45).

Statistical analysis

GraphPad Prism 5.0 (GraphPad Software Inc., San Diego, USA) was used for data graphing and estimating the values of inhibitory concentration 50% (IC50) for any types of cytotoxicity. All experiments were performed with three independent repetitions. Data were showed as mean ± standard deviation (SD)

and were analyzed by factorial analysis of variance (ANOVA) followed by Tukey's post hoc tests. Differences were assessed to be significant p-value was less than 0.05.

Abbreviations

CIS: Cisplatin

PEI: Polyethylenimine

MNPs: Magnetic nanoparticles

MDR: multidrug resistance

Declarations

Ethics approval and consent to participate

Not applicable.

Consent for publication

Not applicable.

Availability of data and materials

All data generated or analyzed during this study are included in this published article and its supplementary information files.

Competing interests

The authors declare that they have no competing interests.

Funding

No funding sources.

Authors' Contributions

F.A. performed the experiments and analyzed the data and also wrote the original draft. B.H.V. and M.S. conceived and designed the study and methodology. P.A. as corresponding author conducted research,

sponsored the study and made all the arrangements. All authors reviewed the final version of the manuscript.

Acknowledgments

The authors would like to thank the Research Council of Tarbiat Modares University for its contributions to this work.

References

1. Sw H, Rz S, Hm J, Kj A-R, As A. The Assessment of Malignant Ovarian Tumors in Baghdadian Women. Prensa Med Argent [Internet]. 2020 [cited 2020 Aug 31];106(1). Available from: https://www.scholarsliterature.com/journals/la-prensa-medica/fulltext/the-assessment-of-malignant-ovarian-tumors-in-baghdadian-women.
2. Perrone MG, Luisi O, De Grassi A, Ferorelli S, Cormio G, Scilimati A. Translational Theragnostic of Ovarian Cancer: Where do we stand? Curr Med Chem [Internet]. 2019 Aug 16 [cited 2020 Sep 1];26. Available from: http://www.eurekaselect.com/174273/article.
3. Mikuš M, Benco N, Matak L, Planinić P, Ćorić M, Lovrić H, et al. Fertility-sparing surgery for patients with malignant ovarian germ cell tumors: 10 years of clinical experience from a tertiary referral center. Arch Gynecol Obstet. 2020 May;301(5):1227–33.
4. Dasari S, Tchounwou PB. Cisplatin in cancer therapy: molecular mechanisms of action. Eur J Pharmacol. 2014;740:364–378.
5. A randomized clinical trial of cisplatin/paclitaxel versus carboplatin/paclitaxel as first-line treatment of ovarian cancer. J Natl Cancer Inst. 2003;95(17):1320–1329.
6. Bertolini G, Roz L, Perego P, Tortoreto M, Fontanella E, Gatti L, et al. Highly tumorigenic lung cancer CD133+ cells display stem-like features and are spared by cisplatin treatment. Proc Natl Acad Sci. 2009;106(38):16281–16286.
7. Fuertes MA, Castilla J, Alonso C, Prez JM. Cisplatin biochemical mechanism of action: from cytotoxicity to induction of cell death through interconnections between apoptotic and necrotic pathways. Curr Med Chem. 2003;10(3):257–266.
8. Baruah H, Rector CL, Monnier SM, Bierbach U. Mechanism of action of non-cisplatin type DNA-targeted platinum anticancer agents: DNA interactions of novel acridinylthioureas and their platinum conjugates. Biochem Pharmacol. 2002;64(2):191–200.
9. McMullen M, Madariaga A, Lheureux S. New approaches for targeting platinum-resistant ovarian cancer. Semin Cancer Biol. 2020 Aug;S1044579X20301863.
10. Galluzzi L, Senovilla L, Vitale I, Michels J, Martins I, Kepp O, et al. Molecular mechanisms of cisplatin resistance. Oncogene. 2012 Apr;31(15):1869–83.

11. Pabla N, Murphy RF, Liu K, Dong Z. The copper transporter Ctr1 contributes to cisplatin uptake by renal tubular cells during cisplatin nephrotoxicity. Am J Physiol-Ren Physiol. 2009;296(3):F505–F511.
12. Samimi G. Increased Expression of the Copper Efflux Transporter ATP7A Mediates Resistance to Cisplatin, Carboplatin, and Oxaliplatin in Ovarian Cancer Cells. Clin Cancer Res. 2004 Jul 15;10(14):4661–9.
13. Rabik CA, Dolan ME. Molecular mechanisms of resistance and toxicity associated with platinating agents. Cancer Treat Rev. 2007;33(1):9–23.
14. Korita PV, Wakai T, Shirai Y, Matsuda Y, Sakata J, Takamura M, et al. Multidrug resistance-associated protein 2 determines the efficacy of cisplatin in patients with hepatocellular carcinoma. Oncol Rep. 2010;23(4):965–972.
15. Materna V, Liedert B, Thomale J, Lage H. Protection of platinum–DNA adduct formation and reversal of cisplatin resistance by anti-MRP2 hammerhead ribozymes in human cancer cells. Int J Cancer. 2005;115(3):393–402.
16. Nies AT, König J, Pfannschmidt M, Klar E, Hofmann WJ, Keppler D. Expression of the multidrug resistance proteins MRP2 and MRP3 in human hepatocellular carcinoma. Int J Cancer. 2001;94(4):492–499.
17. Borst P, Evers R, Kool M, Wijnholds J. A Family of Drug Transporters: the Multidrug Resistance-Associated Proteins. JNCI J Natl Cancer Inst. 2000 Aug 16;92(16):1295–302.
18. Meijer C, Mulder NH, Timmer-Bosscha H, Sluiter WJ, Meersma GJ, de Vries EG. Relationship of cellular glutathione to the cytotoxicity and resistance of seven platinum compounds. Cancer Res. 1992;52(24):6885–6889.
19. Bedford P, Walker MC, Sharma HL, Perera A, McAuliffe CA, Masters JR, et al. Factors influencing the sensitivity of two human bladder carcinoma cell lines to cis-diamminedichloro-platinum (II). Chem Biol Interact. 1987;61(1):1–15.
20. Jansen BA, Brouwer J, Reedijk J. Glutathione induces cellular resistance against cationic dinuclear platinum anticancer drugs. J Inorg Biochem. 2002;89(3–4):197–202.
21. Krieger ML, Eckstein N, Schneider V, Koch M, Royer H-D, Jaehde U, et al. Overcoming cisplatin resistance of ovarian cancer cells by targeted liposomes in vitro. Int J Pharm. 2010 Apr;389(1–2):10–7.
22. Kuo MT, Fu S, Savaraj N, Chen HHW. Role of the Human High-Affinity Copper Transporter in Copper Homeostasis Regulation and Cisplatin Sensitivity in Cancer Chemotherapy. Cancer Res. 2012 Sep 15;72(18):4616–21.
23. Li Y-Q, Yin J-Y, Liu Z-Q, Li X-P. Copper efflux transporters ATP7A and ATP7B: Novel biomarkers for platinum drug resistance and targets for therapy: ATP7A/7B AND PLATINUM DRUG RESISTANCE. IUBMB Life. 2018 Mar;70(3):183–91.
24. Ghasemi M, Sivaloganathan S. A computational study of combination HIFU–chemotherapy as a potential means of overcoming cancer drug resistance. Math Biosci. 2020 Nov;329:108456.

25. Jiang W, Xia J, Xie S, Zou R, Pan S, Wang Z, et al. Long non-coding RNAs as a determinant of cancer drug resistance: Towards the overcoming of chemoresistance via modulation of lncRNAs. Drug Resist Updat. 2020 May;50:100683.
26. Zhang Z, Xie Z, Sun G, Yang P, Li J, Yang H, et al. Reversing drug resistance of cisplatin by hsp90 inhibitors in human ovarian cancer cells. :15.
27. Ai Z, Lu Y, Qiu S, Fan Z. Overcoming cisplatin resistance of ovarian cancer cells by targeting HIF-1-regulated cancer metabolism. Cancer Lett. 2016 Apr;373(1):36–44.
28. Hu C-MJ, Zhang L. Nanoparticle-based combination therapy toward overcoming drug resistance in cancer. Biochem Pharmacol. 2012 Apr;83(8):1104–11.
29. Wang H, Huang Y. Combination therapy based on nano codelivery for overcoming cancer drug resistance. Med Drug Discov. 2020 Jun;6:100024.
30. Chang P-Y, Peng S-F, Lee C-Y, Lu C-C, Tsai S-C, Shieh T-M, et al. Curcumin-loaded nanoparticles induce apoptotic cell death through regulation of the function of MDR1 and reactive oxygen species in cisplatin-resistant CAR human oral cancer cells. Int J Oncol. 2013 Oct;43(4):1141–50.
31. Navarro G, Sawant RR, Biswas S, Essex S, Tros de Ilarduya C, Torchilin VP. P-glycoprotein silencing with siRNA delivered by DOPE-modified PEI overcomes doxorubicin resistance in breast cancer cells. Nanomed. 2012 Jan;7(1):65–78.
32. Abdallah B, Hassan A, Benoist C, Goula D, Behr JP, Demeneix BA. A powerful nonviral vector for in vivo gene transfer into the adult mammalian brain: polyethylenimine. Hum Gene Ther. 1996;7(16):1947–1954.
33. Rhaese S, von Briesen H, Rübsamen-Waigmann H, Kreuter J, Langer K. Human serum albumin–polyethylenimine nanoparticles for gene delivery. J Controlled Release. 2003;92(1–2):199–208.
34. Meng H, Liong M, Xia T, Li Z, Ji Z, Zink JI, et al. Engineered design of mesoporous silica nanoparticles to deliver doxorubicin and P-glycoprotein siRNA to overcome drug resistance in a cancer cell line. ACS Nano. 2010;4(8):4539–4550.
35. Urban-Klein B, Werth S, Abuharbeid S, Czubayko F, Aigner A. RNAi-mediated gene-targeting through systemic application of polyethylenimine (PEI)-complexed siRNA in vivo. Gene Ther. 2005 Mar;12(5):461–6.
36. Yang Y-P, Chien Y, Chiou G-Y, Cherng J-Y, Wang M-L, Lo W-L, et al. Inhibition of cancer stem cell-like properties and reduced chemoradioresistance of glioblastoma using microRNA145 with cationic polyurethane-short branch PEI. Biomaterials. 2012 Feb;33(5):1462–76.
37. Jalali A, Zafari J, Jouni FJ, Abdolmaleki P, Shirazi FH, Khodayar MJ. Combination of static magnetic field and cisplatin in order to reduce drug resistance in cancer cell lines. Int J Radiat Biol. 2019 Aug 3;95(8):1194–201.
38. Ghodbane S, Lahbib A, Sakly M, Abdelmelek H. Bioeffects of Static Magnetic Fields: Oxidative Stress, Genotoxic Effects, and Cancer Studies. BioMed Res Int. 2013;2013:1–12.
39. Ghandoor HE, Zidan HM, Khalil MMH, Ismail MIM. Synthesis and Some Physical Properties of Magnetite (Fe3O4) Nanoparticles. Int J Electrochem Sci. 2012;7:12.

40. Jawad AS, Al-Alawy AF. Synthesis and characterization of coated magnetic nanoparticles and its application as coagulant for removal of oil droplets from oilfield produced water. In Baghdad, Iraq; 2020 [cited 2020 Aug 31]. p. 020174. Available from: http://aip.scitation.org/doi/abs/10.1063/5.0000279
41. Frost RL, Palmer SJ, Xi Y, Čejka J, Sejkora J, Plášil J. Spectrochimica acta. Part A, Molecular and biomolecular spectroscopy 61. 2005;
42. Hajipour Verdom B, Abdolmaleki P, Behmanesh M. The Static Magnetic Field Remotely Boosts the Efficiency of Doxorubicin through Modulating ROS Behaviors. Sci Rep. 2018 Dec;8(1):990.
43. An JJ, Shi KJ, Wei W, Hua FY, Ci YL, Jiang Q, et al. The ROS/JNK/ATF2 pathway mediates selenite-induced leukemia NB4 cell cycle arrest and apoptosis in vitro and in vivo. Cell Death Dis. 2013 Dec;4(12):e973–e973.
44. Riccardi C, Nicoletti I. Analysis of apoptosis by propidium iodide staining and flow cytometry. Nat Protoc. 2006 Aug;1(3):1458–61.
45. Shapiro HM. Practical flow cytometry. John Wiley & Sons; 2005.
46. Tseng C-L, Yang K-C, Yen K-C, Yueh-Hsiu Wu S, Lin F-H. Preparation and Characterization of Cisplatin-Incorporated Gelatin Nanocomplex for Cancer Treatment. Curr Nanosci. 2011 Dec 1;7(6):932–7.
47. Mainini F, Eccles MR. Lipid and Polymer-Based Nanoparticle siRNA Delivery Systems for Cancer Therapy. Molecules. 2020 Jun 10;25(11):2692.
48. Yang T, Du G, Cui Y, Yu R, Hua C, Tian W, et al. pH-sensitive doxorubicin-loaded polymeric nanocomplex based on β-cyclodextrin for liver cancer-targeted therapy. Int J Nanomedicine. 2019;14:1997–2010.
49. Lim WQ, Phua SZF, Zhao Y. Redox-Responsive Polymeric Nanocomplex for Delivery of Cytotoxic Protein and Chemotherapeutics. ACS Appl Mater Interfaces. 2019 Sep 4;11(35):31638–48.
50. Marullo R, Werner E, Degtyareva N, Moore B, Altavilla G, Ramalingam SS, et al. Cisplatin induces a mitochondrial-ROS response that contributes to cytotoxicity depending on mitochondrial redox status and bioenergetic functions. PloS One. 2013;8(11):e81162.
51. Khansarizadeh M, Mokhtarzadeh A, Rashedinia M, Taghdisi SM, Lari P, Abnous KH, et al. Identification of possible cytotoxicity mechanism of polyethylenimine by proteomics analysis. Hum Exp Toxicol. 2016;35(4):377–387.
52. Chen HHW, Kuo MT. Role of Glutathione in the Regulation of Cisplatin Resistance in Cancer Chemotherapy. Met-Based Drugs. 2010;2010:1–7.
53. Karimi F, Fallah Shojaei A, Tabatabaeian K, Karimi-Maleh H, Shakeri S. HSA loaded with CoFe2O4/MNPs as a high-efficiency carrier for epirubicin anticancer drug delivery. IET Nanobiotechnol. 2018 Apr 1;12(3):336–42.
54. Basu A, Krishnamurthy S. Cellular responses to Cisplatin-induced DNA damage. J Nucleic Acids. 2010;2010.

55. Goodarzi AA, Noon AT, Deckbar D, Ziv Y, Shiloh Y, Löbrich M, et al. ATM signaling facilitates repair of DNA double-strand breaks associated with heterochromatin. Mol Cell. 2008;31(2):167–177.
56. Zhang Y, Qian D, Li Z, Huang Y, Wu Q, Ru G, et al. Oxidative stress-induced DNA damage of mouse zygotes triggers G2/M checkpoint and phosphorylates Cdc25 and Cdc2. Cell Stress Chaperones. 2016;21(4):687–696.
57. Valko M, Rhodes Cj, Moncol J, Izakovic MM, Mazur M. Free radicals, metals and antioxidants in oxidative stress-induced cancer. Chem Biol Interact. 2006;160(1):1–40.
58. Cao X, Hou J, An Q, Assaraf YG, Wang X. Towards the overcoming of anticancer drug resistance mediated by p53 mutations. Drug Resist Updat. 2020 Mar;49:100671.
59. Chen L, Chen C, Wang P, Song T. Mechanisms of cellular effects directly induced by magnetic nanoparticles under magnetic fields. J Nanomater. 2017;2017.
60. Peklak-Scott C, Smitherman PK, Townsend AJ, Morrow CS. Role of glutathione *S*-transferase P1-1 in the cellular detoxification of cisplatin. Mol Cancer Ther. 2008 Oct;7(10):3247–55.
61. Bernareggi A, Torti L, Maffei Facino R, Carini M, Depta G, Casetta B, et al. Characterization of cisplatin-glutathione adducts by liquid chromatography-mass spectrometry evidence for their formation in vitro but not in vivo after concomitant administration of cisplatin and glutathione to rats and cancer patients. J Chromatogr B Biomed Sci App. 1995 Jul;669(2):247–63.
62. Bodega G, Alique M, Puebla L, Carracedo J, Ramírez RM. Microvesicles: ROS scavengers and ROS producers. J Extracell Vesicles. 2019 Dec 1;8(1):1626654.
63. Boussif O, Lezoualc'h F, Zanta MAntoniet, Mergny MD, Scherman D, Demeneix B, et al. A versatile vector for gene and oligonucleotide transfer into cells in culture and in vivo: polyethylenimine. Proc Natl Acad Sci. 1995;92(16):7297–7301.
64. Benjaminsen RV, Mattebjerg MA, Henriksen JR, Moghimi SM, Andresen TL. The Possible "Proton Sponge " Effect of Polyethylenimine (PEI) Does Not Include Change in Lysosomal pH. Mol Ther. 2013 Jan;21(1):149–57.

Tables

Due to technical limitations, tables are only available as a download in the Supplemental Files section.

Figures

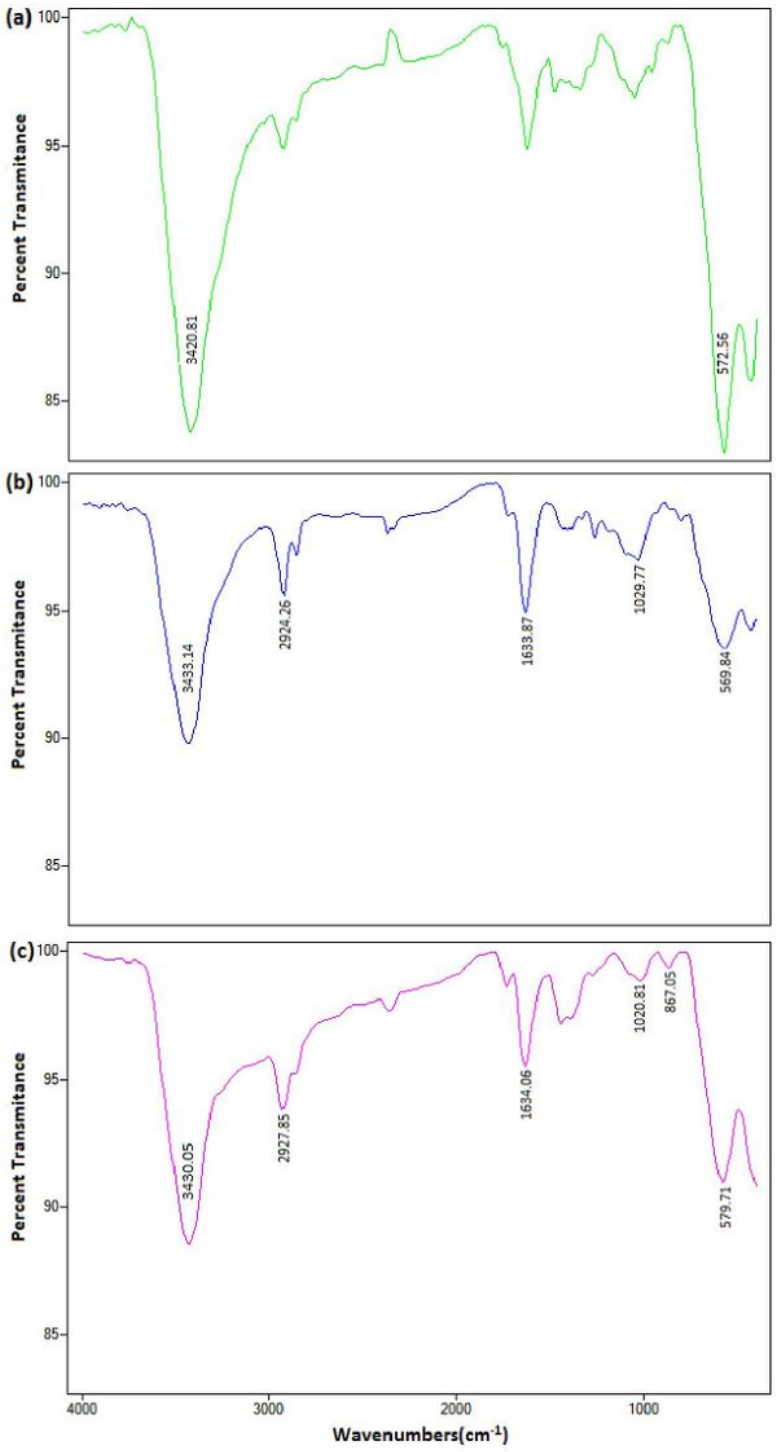

Figure 1

The FTIR spectrum of (a) MNPs, (b) PEI-MNPs (PM) and (c) PEI-MNP-CIS (PMC) in the range of 400-4000 cm-1 wavelengths. The FTIR spectrum of MNPs is visible on two peaks. The first absorption pic is in the range of 3420 cm-1 wavelength that is related to the hydration bond formed with hydroxyl groups and second absorption pic is within the range of 572 cm-1, which is due to the vibrational band of Fe-O in the nanoparticles. These peaks confirm the accuracy of nanoparticle synthesis. In the PM binary complex, in

addition to MNPs-dependent peaks (3433 and 569 cm-1), the wavelengths of 2924, 1633, and 1029 cm-1 indicate C-H, C-C, and C-N bonds of PEI polymer, respectively. These results confirmed the accuracy of PM binary complex formation. In the PMC ternary complex spectrum, in addition the peaks of MNP and PM, peaks are in the range of 867 cm-1, which indicated the N-H bond of the cisplatin drugs.

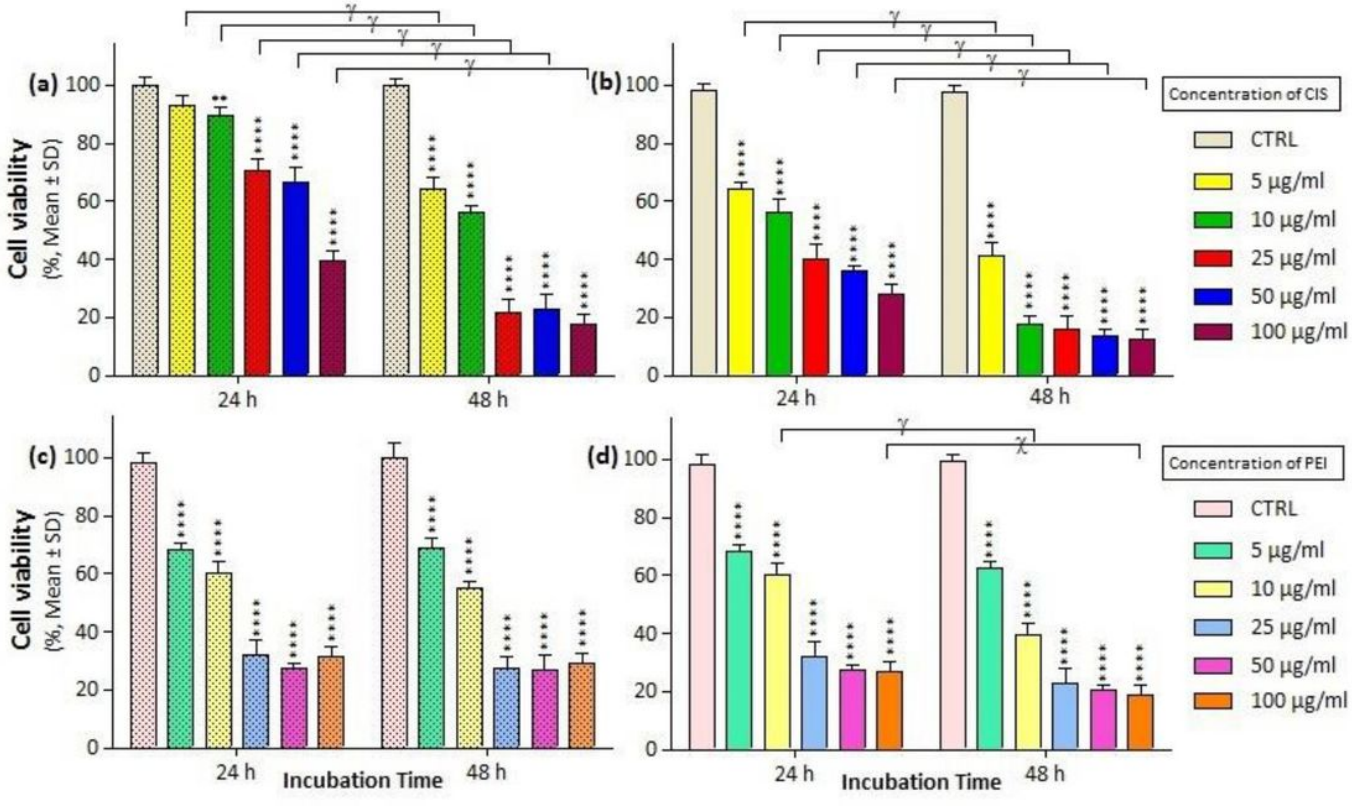

Figure 2

The cell viability results of (a, c) A2780/CP and (b, d) A2780 cells treated with cisplatin (CIS) and polyethylenimine (PEI) at the same different concentrations (5, 10, 25, 50 and 100 µg/ml) for two exposure times (24 and 48 h), respectively. Cell viability values were determined by MTT assay and microplate reader, and results are expressed as the percentage of viable cells. Data are shown as mean ± SD (n = 3). **P<0.01; ****P<0.0001 show significant differences relative to unexposed cells (CTRL), and letters (χ,P<0.001; γ,P <0.0001 show significant differences between treated cells (6 × 2 factorial ANOVA flowed by post-hoc Newman–Keuls multiple comparison tests).

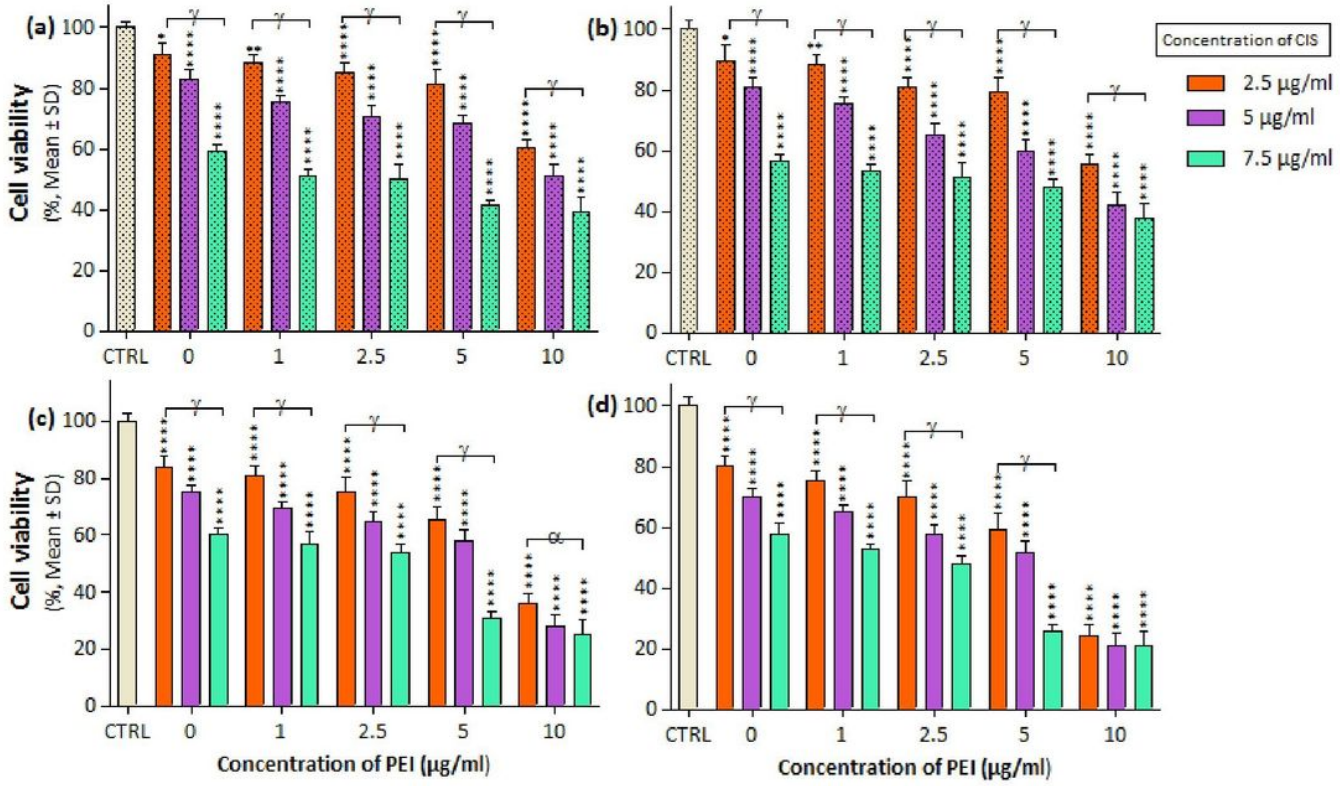

Figure 3

The cell viability results of (a, b) A2780/CP and (c, d) A2780 cells treated with PC binary complexes involves different concentrations of 1, 2/5, 5 and 10 µg/ml polyethylenimine (PEI), and 2.5, 5 and 7.5 µg/ml cisplatin (CIS) for two exposure times (24 and 48 h), respectively. Cell viability values were determined by MTT assay and microplate reader, and results are expressed as the percentage of viable cells. Data are shown as mean ± SD (n = 3). *P<0.05; **P<0.01; ****P<0.0001 show significant differences relative to unexposed cells (CTRL), and letters (γ,P <0.0001) show significant differences between treated cells (5 × 4 factorial ANOVA flowed by post-hoc Newman–Keuls multiple comparison tests).

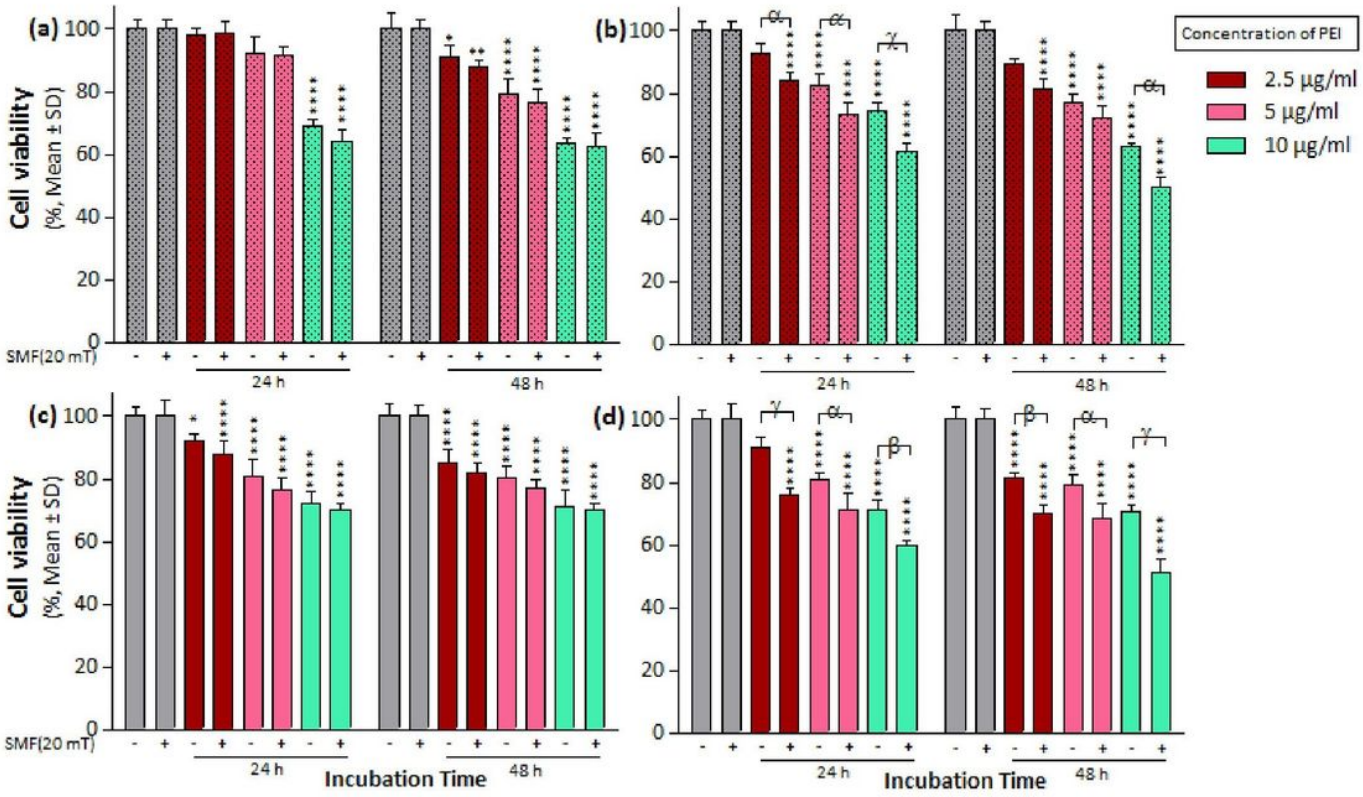

Figure 4

The cell viability results of SMF (20 mT) exposure on (a, b) A2780/CP and (c, d) A2780 cells treated with different concentrations of 2.5, 5 and 10 µg/ml polyethylenimine (PEI) and 1 µg/ml magnetite nanoparticles (MNPs) for two exposure times (24 and 48 h), respectively. Cell viability value was determined by MTT assay and microplate reader, and results are expressed as the percentage of viable cells. Data are shown as mean ± SD (n = 3). *P<0.05; ** P<0.01; ****P<0.0001 show significant differences relative to unexposed cells (CTRL), and letters (α,P<0.05; β,P<0.01 χ,P<0.001; γ,P <0.0001) show significant differences between treated cells (4 × 2 × 2 factorial ANOVA flowed by post-hoc Newman–Keuls multiple comparison tests).

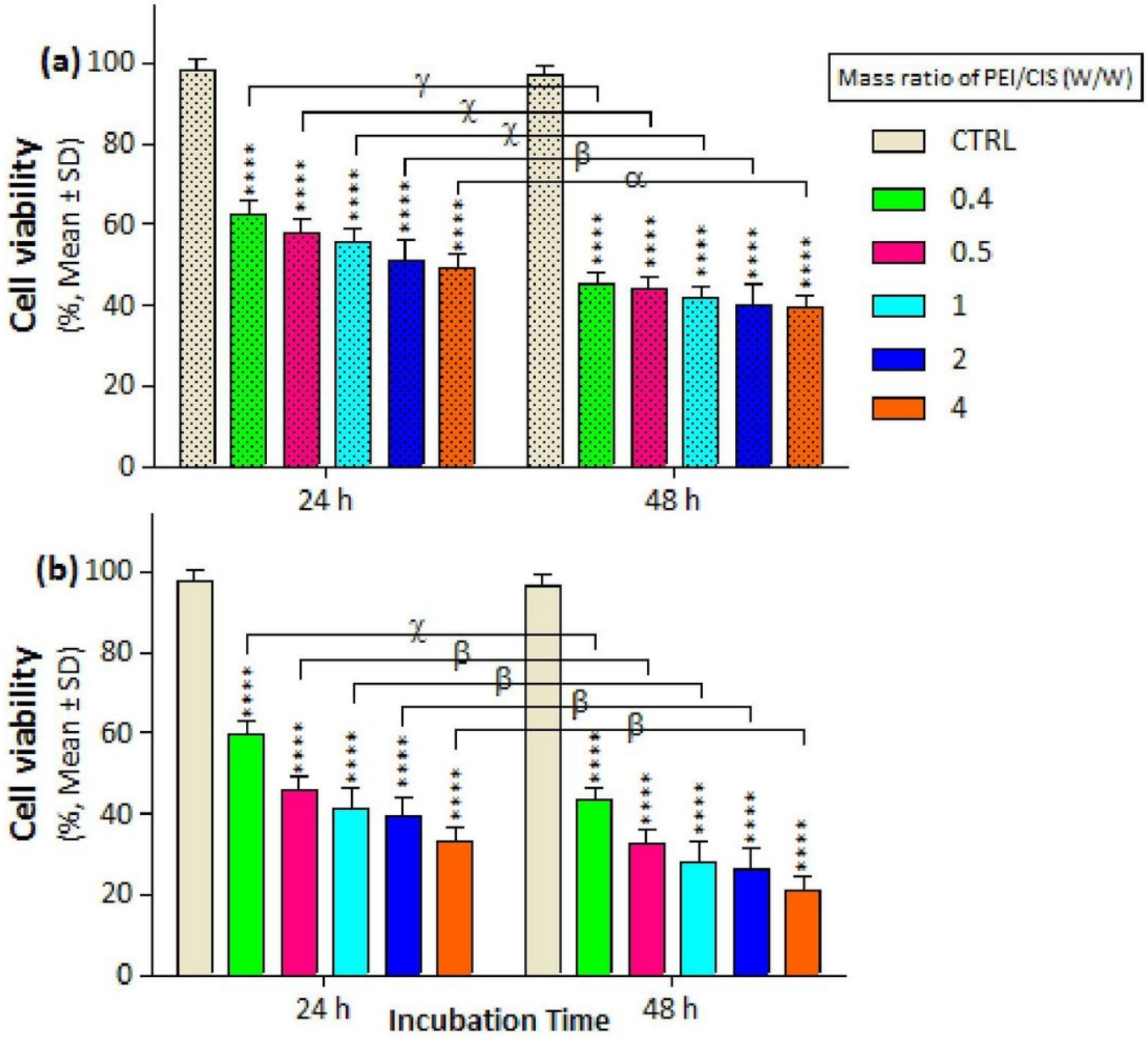

Figure 5

The cell viability results of (a) A2780/CP and (b) A2780 cells treated with three-component magnetic nanocomplex (PEI-MNP-CIS (PMC)) including different mass ratios (0, 0.4, 0.5, 1, 2 and 4 w/w) of polyethylenimine (PEI) compared to cisplatin (CIS) at same concentration 1 μg/ml of Fe3O4 magnetite nanoparticles (MNPs) for two exposure times (24 and 48 h), respectively. Cell viability values were determined by MTT assay and microplate reader, and results are expressed as the percentage of viable cells. Data are shown as mean ± SD (n = 3). ****P<0.0001 show significant differences relative to unexposed cells (CTRL), and letters (α,P<0.05; β,P<0.01; χ,P<0.001; γ,P <0.0001) show significant differences between treated cells (6 × 2 factorial ANOVA flowed by post-hoc Newman–Keuls multiple comparison tests).

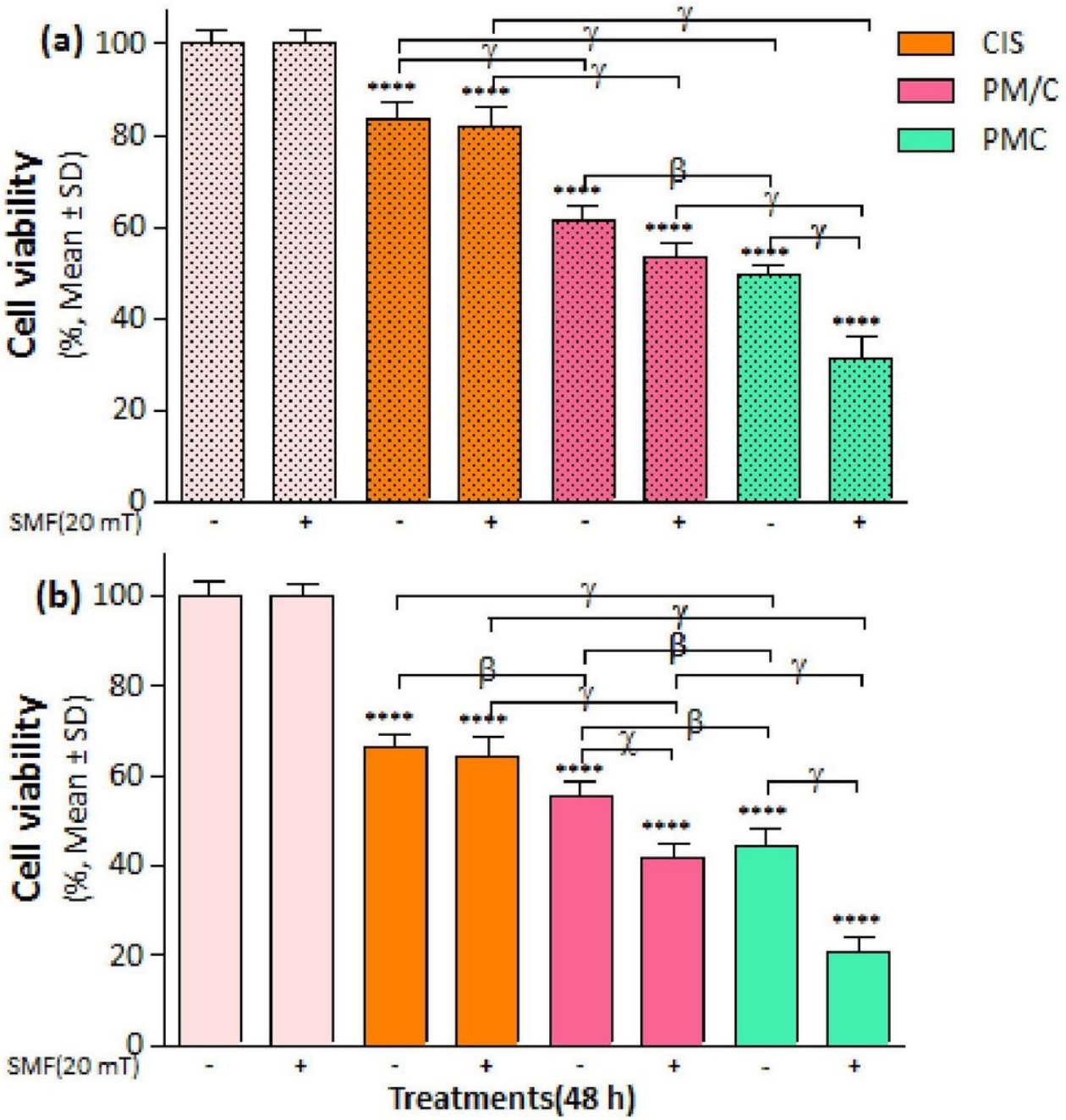

Figure 6

The cell viability results of (a) A2780/CP and (b) A2780 cells treated with (PEI-MNPs/CIS (PM/C)) consist of cisplatin (CIS)-treatment (2.5 µg/ml) after 1 h of PEI-MNPs(PM) binary complex treatment at concentrations of 1 µg/ml polyethylenimine (PEI) and 1 µg/ml Fe3O4 magnetite nanoparticles (MNPs), and also three-component magnetic nanocomplex (PEI-MNP-CIS (PMC)) at the same concentrations of PM/C in presence and absence of 20 mT static magnetic field (SMF) for 48 h . Cell viability values were determined by MTT assay and microplate reader, and results are expressed as the percentage of viable cells. Data are shown as mean ± SD (n = 3).****P<0.0001 show significant differences relative to

unexposed cells (CTRL), and letters (β,P<0.01; χ,P<0.001; γ,P <0.0001 show significant differences between treated cells (2 × 2 × 2 × 2 factorial ANOVA flowed by post-hoc Newman–Keuls multiple comparison tests).

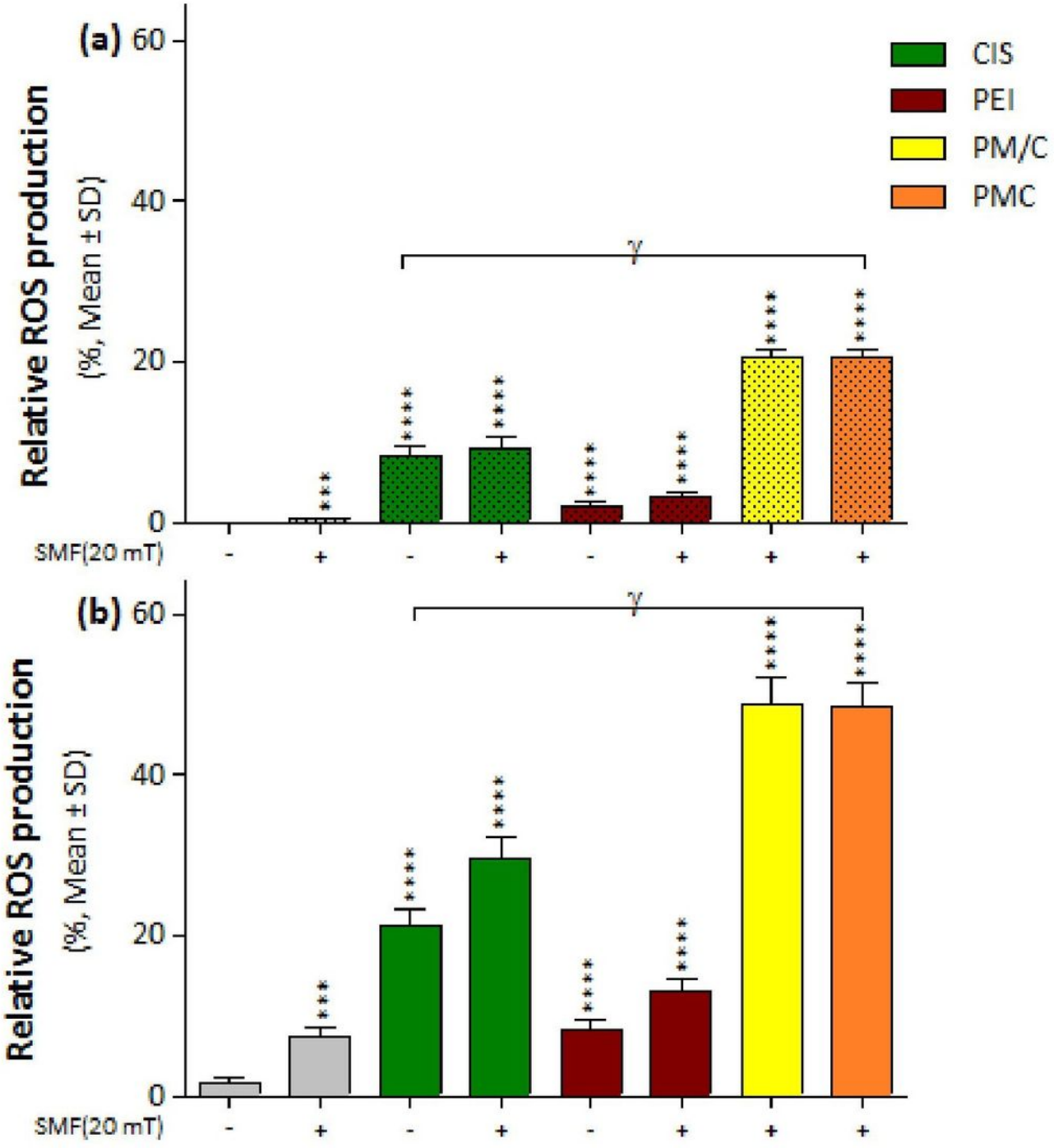

Figure 7

The intracellular ROS generation of (a) A2780/CP and (b) A2780 cells treated to 1 μg/ml of polyethylenimine (PEI), 2.5 μg/ml of cisplatin (CIS), and PM/C and PMC three-component magnetic

nanocomplexes at same concentrations (1 µg/ml PEI, 1 µg/ml MNPs and 2.5 µg/ml CIS) in presence and absence of 20 mT static magnetic field (SMF) for 48 h. Cells were collected and the ROS generation was evaluated by using oxidized DCFDA and Flow-Cytometry analysis. Data are shown as mean ± SD (n = 3). ***P<0.001; ****P<0.0001 show significant differences relative to unexposed cells (CTRL), and letters (α,P<0.05; χ,P<0.001; γ,P <0.0001 show significant differences between treated cells (2 × 2 × 2 × 2 × 2 factorial ANOVA flowed by post-hoc Newman–Keuls multiple comparison tests).

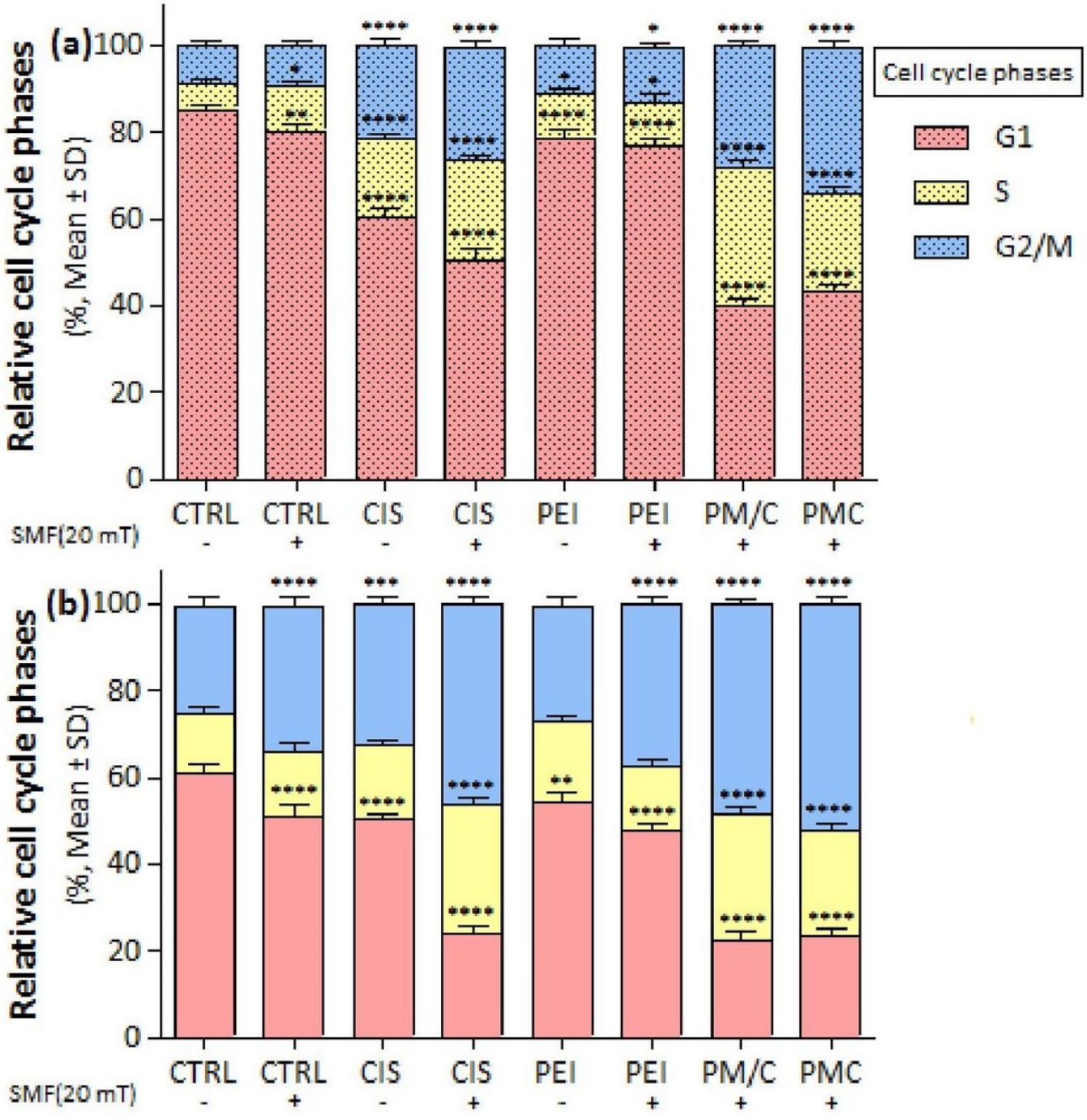

Figure 8

The cell cycle arrest of (a) A2780/CP and (b) A2780 cells treated to 1 μg/ml of polyethylenimine (PEI), 2.5 μg/ml of cisplatin (CIS), and PM/C and PMC three-component magnetic nanocomplexes at same concentrations (1 μg/ml PEI, 1 μg/ml MNPs and 2.5 μg/ml CIS) in presence and absence of 20 mT static magnetic field (SMF) for 48 h. Cells were analyzed for cell cycle distribution through propidium iodide flow cytometry kit. The plot shows cells in G1, S and G2/M phases. Data are shown as mean ± SD (n = 3). *P<0.05; **P<0.01 ***P<0.001; ****P<0.0001 show significant differences relative to unexposed cells (CTRL). (2 × 2 × 2 × 2 × 2 factorial ANOVA flowed by post-hoc Newman–Keuls multiple comparison tests).

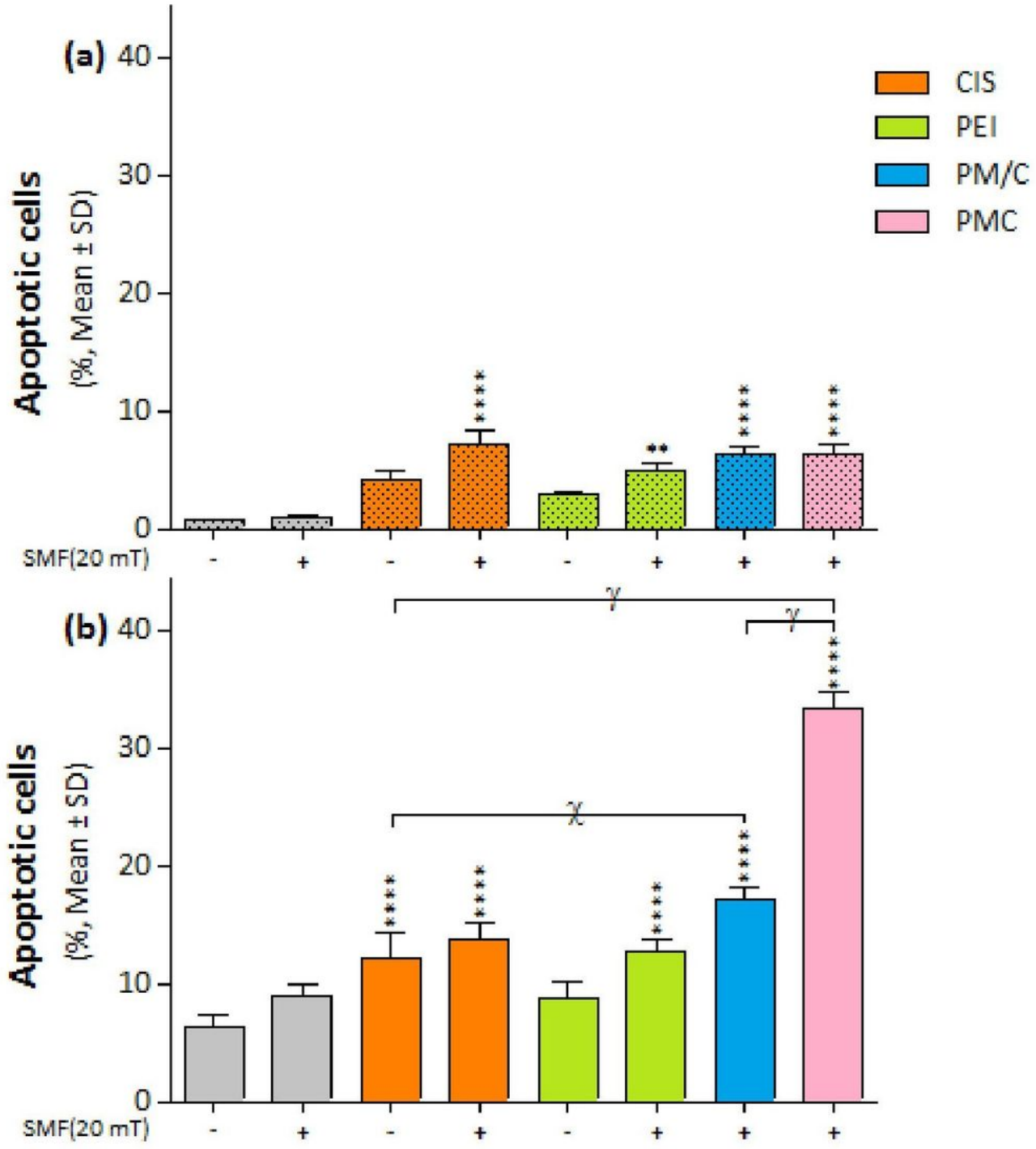

Figure 9

The apoptosis cell death of (a) A2780/CP and (b) A2780 cells treated to 1 μg/ml of polyethylenimine (PEI), 2.5 μg/ml of cisplatin (CIS), and PM/C and PMC three-component magnetic nanocomplexes at same concentrations (1 μg/ml PEI, 1 μg/ml MNPs and 2.5 μg/ml CIS) in presence and absence of 20 mT static magnetic field (SMF) for 48 h. Cells were collected and labeled with annexin V/PI for flow cytometric analysis. The bar graphs represented the mean values of the apoptotic cells (Q2+Q3). Data are

shown as mean ± SD (n = 3). **P<0.01; ****P<0.0001 show significant differences relative to unexposed cells (CTRL), and letters (χ,P<0.001; γ,P <0.0001 show significant differences between treated cells (2 × 2 × 2 × 2 × 2 factorial ANOVA flowed by post-hoc Newman–Keuls multiple comparison tests).

Supplementary Files

This is a list of supplementary files associated with this preprint. Click to download.

- Supplementarymaterial.docx
- Tables.docx